Journal of Sound and Vibration 327 (2009) 121–133

Contents lists available at ScienceDirect

Journal of Sound and Vibration

journal homepage: www.elsevier.com/locate/jsvi

Large amplitude motion mechanism and non-planar vibration character of stay cables subject to the support motions

Lianhua Wang [a,b,*], Yueyu Zhao [a]

[a] College of Civil Engineering, Hunan University, Changsha, Hunan 410082, PR China
[b] Key Laboratory of Building Safety and Energy Efficiency, Ministry of Education, PR China

ARTICLE INFO

Article history:
Received 23 September 2008
Received in revised form
3 April 2009
Accepted 11 June 2009
Handling Editor: L.G. Tham
Available online 8 July 2009

ABSTRACT

In this study, the shooting method and the continuation technique are applied to investigate the large amplitude motion and non-planar motion characteristic of the inclined cable subject to the support motion. Considering the geometric nonlinearity and the quasi-static assumption, a spatial discrete model of the cable is formulated, which is used to determine the frequency–response curves of the cable. The effects of the amplitude of the support motion and the inclined angle on the coupling motion of the inclined cable are investigated. It is shown that the coupling motion may occur, and the motions play a noticeable role on the axial tensions of the cable. Also, the non-periodic spatial motions of the cable are examined through direct simulations.

1. Introduction

Due to their economic design and esthetic appearance, stay cables are very efficient structural components in cable-stayed bridges. However, owing to their large flexibility, relatively small mass and extremely low inherent damping, cables are often susceptible to exhibit large amplitude vibration due to the motion of the bridge deck and towers. Because large-amplitude vibrations of cables play an important role in the undue stresses and fatigue in the anchorage at the deck or tower and in the cables themselves, this kind of large amplitude vibration of stay cables have been extensively investigated in the past decade [1].

Cai and Chen [2] applied the numerical simulation to investigate the nonlinear response of the inclined cable subject to parametric and external resonances. Lilien and Pinto da Costa [3] investigated the large amplitude vibrations of stay cable due to the parametric excitation. Pinto da Costa et al. [4] studied the oscillations of stay cables due to periodic motions of the girder or pylon. Berlioz and Lamarque [5] made the theoretical and experimental investigations of an inclined cable subject to the boundary motion condition, and they also presented a simple cable model to study nonlinear oscillation. Georgakis and Taylor [6] investigated the nonlinear dynamics of cable stays, induced by sinusoidal cable-plane structural vibrations. Recently, based on the LQR control and the Bingham model of MR dampers, Ying et al. [7] developed a semi-active optimal control method for stay cables to studied the instability of controlled inclined stay cables under support motions. Although the support motions may result in the large-amplitude vibrations, the axial support motion can also generate a control force [8].

* Corresponding author at: College of Civil Engineering, Hunan University, Changsha, Hunan 410082, PR China. Tel.: +86 731 8823962; fax: +86 731 8822029.
E-mail addresses: Lhwang@hnu.cn, Wanglianhua1975@yahoo.com (L. Wang).

0022-460X/$ - see front matter © 2009 Elsevier Ltd. All rights reserved.
doi:10.1016/j.jsv.2009.06.013

In recent years, the wide applications of cable-stayed bridge systems have attracted increasing attention on the modal interactions of cable-stayed beam [9–15], where the nonlinear interaction between the global modes and local modes has been addressed. Furthermore, Caetano et al. [16] applied the on-site measurement results and a 3-D finite element model of the Guadiana Bridge to investigate the different cable–deck interaction of the bridge under environmental excitations. Their results showed that the one-to-one resonance condition between global and local modes can lead to the linear interaction and a modal shape distortion. The on-site measurement results also showed that the cable–deck interaction may excite the large amplitude vibration of stay cable through the support motion produced by the deck vibration. These researches deepen our understanding on the excitation mechanism of the large amplitude of stay cables caused by deck and/or tower motions.

In general, the single-degree-of-freedom (sdof) cable model is widely applied in the most previous studies. However, this kind of model cannot be used to investigate the spatial finite oscillations of cables due to their overall flexibility. Therefore, it ignores some inherent prosperities such as the overall flexibility. Moreover, any nonlinear interactions among all the modes, directly or indirectly excited, can not be considered. Therefore, a more accurate spatial discrete model is desired in order to capture the dynamic characteristics and reflect the overall flexibility. Generally speaking, a single-mode Galerkin discretization may lead to significant quantitative or even qualitative errors. Therefore, the multi-mode discrete models were applied to investigate the nonlinear vibration of suspended cable with the help of the continuation technique [17,18]. However, these studies only focused on the direct external excitation, the results did not show the nonlinear character of the stay cables subject to the support motion.

In the present paper, the large-amplitude vibration of the inclined cable subject to the support motions is investigated. Applying the Hamilton principle, the nonlinear governing equations of the cable are derived. The bending, torsional and shear rigidities are neglected. Then, multi-mode expansions of the displacements are applied to obtain a discrete cable model. Numerical analysis are performed by means of the shooting method and the continuation technique. The spatial motion characteristic of the inclined cable is discussed in detail.

2. Mathematical models

As shown in Fig. 1, an inclined homogenous elastic cable subject to a vertical sinusoidal support motion: $Z\sin\omega t$ (where Z and ω denote the amplitude and frequency of the support motion, respectively), is considered. A Cartesian coordinate system $O-xyz$ is chosen, with the origin O placed at the left fixed support of the cable. The solid lines denote the static and dynamic configurations. The displacements of the point are denoted by $u(x,t)$, $v(x,t)$ and $w(x,t)$ along the x, y and z directions, respectively. In the following section, applying the Hamilton principle and the *quasi-static* assumption [19], we will derive a theoretical model that describes the nonlinear vibrations of the inclined cable, where the bending, torsional and shear rigidities of the cable are neglected.

By assuming the Lagrangian strain as the strain measure, the axial Lagrangian strain of the inclined cable can be written as [20]

$$\varepsilon(x,t) = u' + y'v' + \frac{v'^2 + w'^2}{2}, \tag{1}$$

where the prime indicates differentiation with respect to the coordinate x; $y(x)$ is the static configuration of the cable. The equations of motions can be obtained by means of the Hamilton principle,

$$m\ddot{u} + c_u\dot{u} - \left\{EA\left[u' + y'v' + \frac{v'^2 + w'^2}{2}\right]\right\}' = 0, \tag{2}$$

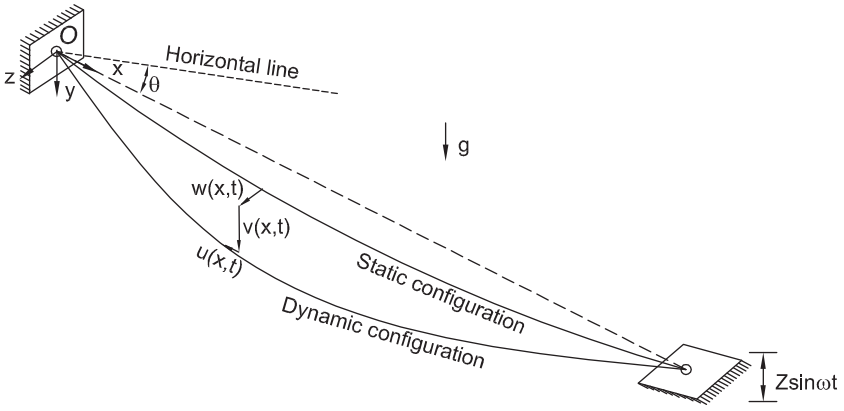

Fig. 1. The theoretical model of the inclined cable subject to the support motion.

$$m\ddot{v} + c_v\dot{v} - \left\{ Hv' + EA(y' + v')\left[u' + y'v' + \frac{v'^2 + w'^2}{2}\right]\right\}' = 0, \tag{3}$$

$$m\ddot{w} + c_w\dot{w} - \left\{ Hw' + EAw'\left[u' + y'v' + \frac{v'^2 + w'^2}{2}\right]\right\}' = 0, \tag{4}$$

where m is the mass per unit length; E is the Young modulus; A is the area of the cross-section; c_u, c_v and c_w are the viscous damping coefficients per unit length; the dot indicates differentiation with respect to time t; H is the axial component of the initial tension and $H \ll EA$ and g is the gravitational acceleration. The boundary conditions can be written as

$$u(0,t) = v(0,t) = w(0,t) = w(l,t) = 0, \quad u(l,t) = Z\sin\theta\sin\omega t, \quad v(l,t) = Z\cos\theta\sin\omega t, \tag{5}$$

where l is the cable span and θ is the inclined angle. Obviously, the boundary conditions of the inclined cable are nonhomogeneous both in the axial displacement component $u(x,t)$ and in-plane transverse displacement component $v(x,t)$. Under the quasi-static assumption, neglecting the acceleration and velocity term in Eq. (2), and taking into account the boundary conditions, the displacement $u(x,t)$ can be expressed by

$$u(x,t) = Z\sin\theta\sin\omega t\frac{x}{l} + \frac{x}{l}\int_0^l \left(y'v' + \frac{v'^2 + w'^2}{2}\right)\mathrm{d}x - \int_0^x \left(y'v' + \frac{v'^2 + w'^2}{2}\right)\mathrm{d}x. \tag{6}$$

Proceeding in a manner similar to Refs. [19,20], the non-dimensional form of the equations of motion of the cable can be written as

$$\ddot{v} + c_v\dot{v} - \frac{\alpha}{\pi^2}(y'' + v'')\left\{ z_0\sin\theta\sin\Omega t + \int_0^1 \left(y'v' + \frac{v'^2 + w'^2}{2}\right)\mathrm{d}x\right\} = 0, \tag{7}$$

$$\ddot{w} + c_w\dot{w} - \frac{\alpha}{\pi^2}w''\left\{ z_0\sin\theta\sin\Omega t + \int_0^1 \left(y'v' + \frac{v'^2 + w'^2}{2}\right)\mathrm{d}x\right\} = 0, \tag{8}$$

where the following non-dimensional variables are introduced,

$$x^* = x/l, \quad y^* = y/l, \quad z_0 = Z/l, \quad v^* = v/l, \quad w^* = w/l, \quad \alpha = EA/H, \quad t^* = t\pi/l\sqrt{H/m},$$

$$\Omega = \omega l/\pi\sqrt{m/H}, \quad c_v^* = c_v l/(\pi m)\sqrt{m/H}, \quad c_w^* = c_w l/(\pi m)\sqrt{m/H}. \tag{9}$$

Also, the asterisks in Eqs. (7) and (8) are dropped for simplicity.

2.1. Discrete model

For the nonhomogeneous boundary value problem, it is convenient to introduce a suitable chosen particular solution, which satisfies the nonhomogeneous boundary conditions, to transform the nonhomogeneous problem to homogeneous one. Then the solution of homogeneous problem can be described by the Fourier series with the eigenfunctions of the homogeneous problem. In this study, according to the boundary condition of the inclined cable, the non-dimensional displacements $v(x,t)$ and $w(x,t)$ can be expressed by the expansions

$$v(x,t) = \sum_{i=1}^{N}\phi_i(x)q_{iv}(t) + xz_0\cos\theta\sin\Omega t, \quad w(x,t) = \sum_{i=1}^{M}\phi_i(x)q_{iw}(t), \tag{10}$$

where $q_{iv}(t)$ and $q_{iw}(t)$ are the generalized coordinates, and $\phi_i(x) = \sqrt{2}\sin i\pi x$, N and M are the number of retained terms in the sine series. Substitution of Eq. (10) into Eqs. (7) and (8) and application of the Galerkin method yield a set of nonlinear ordinary differential equations

$$\begin{aligned}\ddot{q}_{iv} + 2\omega_{iv}\xi_{iv}\dot{q}_{iv} + \Gamma_{1ij}q_{iv} + \sum_{j=1}^{N}(\Gamma_{2ij}q_{jv} + \Gamma_{3ij}q_{jv}^2 + \Gamma_{4ij}q_{jv}q_{iv} + \Gamma_{5ij}q_{jv}^2q_{iv})\\ + \sum_{j=1}^{M}(\Gamma_{3ij}q_{jw}^2 + \Gamma_{5ij}q_{jw}^2q_{iv}) = \Gamma_{6ij}\sin\Omega t + \Gamma_{7ij}\cos\Omega t + \Gamma_{8ij}\sin^2\Omega t, \quad i = 1,2,\ldots,N,\end{aligned} \tag{11}$$

$$\ddot{q}_{iw} + 2\omega_{iw}\xi_{iw}\dot{q}_{iw} + \Gamma_{1ij}q_{iw} + \sum_{j=1}^{N}\Gamma_{4ij}q_{jv}q_{iw} + \sum_{j=1}^{N}\Gamma_{5ij}q_{jv}^2q_{iw} + \sum_{j=1}^{M}\Gamma_{5ij}q_{jw}^2q_{iv} = 0, \quad i = 1,2,\ldots,M, \tag{12}$$

where the modal damping is used, ξ_{iv} and ξ_{iw} are the viscous damping ratio, ω_{iv} and ω_{iw} are the ith in-plane and out-of-plane natural frequency, respectively. Moreover, the expressions of the other coefficients in Eqs. (11) and (12) are defined in Appendix A. Neglecting any nonlinear, damping and excitation terms in Eqs. (11) and (12), the eigenvalue problem can be applied to determine the in-plane and out-of-plane natural frequencies.

2.2. Static configuration of the inclined cable

Referring to Fig. 1, the vertical static equilibrium of the inclined cable is determined by the following nonlinear equation [21]:

$$Hy'' = -mgl\cos\theta\{1+(\tan\theta+y')^2\}^{1/2}. \tag{13}$$

According to the small sag assumption, the y' is enough small to ignore its square in Eq. (13). The static configuration of the inclined cable can be approximately written as [21]

$$y(x) = \frac{mgl\cos\theta}{2H}x(1-x)\left\{1-\frac{\varepsilon_*}{3}(1-2x)\right\}, \tag{14}$$

where $\varepsilon_* = mgl\sin\theta/H$.

3. Method of solution

In this study, the frequency–response curve (*frc*) of the inclined cable is applied to investigate the spatial motion of the cable. In order to construct the *frc*, firstly, the periodic motion of the cable, governed by Eqs. (11) and (12), should be determined for a given excitation frequency Ω^*. For this purpose, Eqs. (11) and (12) are rearranged in the normal form as a set of first-order equations; that is

$$\dot{\mathbf{y}} = \mathbf{A}\mathbf{y} + \mathbf{F}(\mathbf{y}, \Omega, t), \tag{15}$$

where $\mathbf{y} = \{\dot{\mathbf{q}}^{\mathrm{T}}, \mathbf{q}^{\mathrm{T}}\}^{\mathrm{T}}$ ($\mathbf{q} = \{q_{1v},\ldots,q_{jv},\ldots,q_{Nv},q_{1w},\ldots,q_{jw},\ldots,q_{Mw}\}^{\mathrm{T}}$, and T is the transpose),

$$\mathbf{A} = \begin{bmatrix} -\mathbf{C} & -\mathbf{K} \\ \mathbf{I} & \mathbf{0} \end{bmatrix}_{2(N+M)\times 2(N+M)},$$

$\mathbf{C}$ is the modal damping matrix; $\mathbf{I}$ is the $(N+M)\times(N+M)$ unit matrix; $\mathbf{K}$ is the $(N+M)\times(N+M)$ linear stiffness matrix; $\mathbf{F}(\mathbf{y},\Omega,t) = \{\{\mathbf{K}_2+\mathbf{K}_3+\mathbf{P}(\Omega,t)\}^{\mathrm{T}}, \mathbf{0}^{\mathrm{T}}\}^{\mathrm{T}}$; $\mathbf{K}_2$ and $\mathbf{K}_3$ are the $1\times(N+M)$ vectors of quadratic and cubic nonlinear terms, respectively; $\mathbf{P}$ is the $1\times(N+M)$ vector of excitation terms. To obtain the *frc* of the inclined cable, we firstly determine one periodic solution of the equations of motion (Eq. (15)).

3.1. The shooting method

Generally, the periodic solutions are determined by solving a two-point boundary problem, which can be solved by applying the shooting method [22]. Choosing an initial condition $\mathbf{y}(0) = \boldsymbol{\eta}$, Eq. (15) is integrated by means of the Runge–Kutta method over $[0, T]$. The periodic solution, if one exists, can be found when the residual vector $\mathbf{G}(\boldsymbol{\eta}, \Omega)$ satisfies the following the equation:

$$\mathbf{G}(\boldsymbol{\eta}, \Omega) = \mathbf{y}(\boldsymbol{\eta}, \Omega) - \boldsymbol{\eta} = \mathbf{0}. \tag{16}$$

For a given Ω, Eq. (16) includes $2(N+M)$ nonlinear algebraic equations and $2(N+M)$ unknowns, and can be solved iteratively by using the Newton–Raphson iteration. To obtain the iterative scheme, we expand Eq. (16) in a first-order Taylor series, and obtain

$$\left[\left(\frac{\partial\mathbf{y}}{\partial\boldsymbol{\eta}}\right)^{(i)} - \mathbf{I}\right]\Delta\boldsymbol{\eta}^{(i+1)} = -\mathbf{G}(\boldsymbol{\eta}^{(i)}, \Omega), \tag{17}$$

where the superscripts have been added to indicate the iteration step. From Eq. (17), it is clear that the matrix $\partial\mathbf{y}/\partial\boldsymbol{\eta}$ must be determined at $t = T$. To obtain this matrix, we differentiate both sides of Eq. (15) and the initial condition with respect to $\boldsymbol{\eta}$, and obtain the following equations:

$$\frac{\partial}{\partial t}\left(\frac{\partial\mathbf{y}}{\partial\boldsymbol{\eta}}\right) = \frac{\partial}{\partial\mathbf{y}}(\mathbf{A}\mathbf{y}+\mathbf{F})\frac{\partial\mathbf{y}}{\partial\boldsymbol{\eta}}, \quad \frac{\partial\mathbf{y}}{\partial\boldsymbol{\eta}}(0) = \mathbf{I}. \tag{18}$$

According to the shooting method, if an initial guess $\boldsymbol{\eta}^{(0)}$ of the periodic solution $\boldsymbol{\eta}^*$ for a given $\Omega = \Omega^*$ is chosen, the algorithm for the $(i+1)$th iteration ($i = 0, 1, 2, \ldots$) is:

1. *Numerical integration*: Supply the initial condition $\boldsymbol{\eta}^{(i)}$; integrate Eqs. (15) and (18) simultaneously over $[0, T]$ by applying the Runge–Kutta method.
2. *Obtain correction* $\Delta\boldsymbol{\eta}^{(i+1)}$: Evaluate the matrix and vector appearing in Eq. (17) and solve for the correction $\Delta\boldsymbol{\eta}^{(i+1)}$.

3. *Convergence check*: Test whether $\|\Delta\boldsymbol{\eta}^{(i+1)}\|$(where $\|\cdot\|$ denotes the Euclidian vector norm) satisfies a certain convergence criterion or not. If the convergence criterion is satisfied, the periodic solution $\boldsymbol{\eta}^* = \boldsymbol{\eta}^{(i)}$ has been obtained. If not, the solution is updated (i.e., $\boldsymbol{\eta}^{(i+1)} = \boldsymbol{\eta}^{(i)} + \Delta\boldsymbol{\eta}^{(i+1)}$), and return to Step 1.

Based on the algorithm mentioned above, a *Mathematica* code is developed to seek the periodic solution of Eq. (15) in this study. Moreover, the eigenvalues of the matrix $\partial\mathbf{y}/\partial\boldsymbol{\eta}|_{\boldsymbol{\eta}^*}$ are used to determine the stability of the periodic solutions. The stability of the periodic solution is classified as follows: if the maximum eigenvalue lies inside the unit circle in the complex plane, the periodic solution is stable, otherwise the periodic solution is unstable.

3.2. The continuation technique

After the periodic solution $\boldsymbol{\eta}^*$ at $\Omega = \Omega^*$ is determined, the continuation technique [22] can be used to determine the frequency–response curves of the suspended cable as the non-dimensional excitation frequency Ω changes. In this spirit, we introduce the arc-length parameter s as an independent variable and consider the parameter Ω as an unknown variable as well, so that $\boldsymbol{\eta} \equiv \boldsymbol{\eta}(s)$, $\Omega \equiv \Omega(s)$. From Eq. (16), we can obtain

$$\left(\frac{\partial\mathbf{y}}{\partial\boldsymbol{\eta}} - \mathbf{I}\right)\frac{\partial\boldsymbol{\eta}}{\partial s} + \frac{\partial\mathbf{y}}{\partial\Omega}\frac{\partial\Omega}{\partial s} = 0. \tag{19}$$

Similar to the shooting method, we should evaluate the matrix $\partial\mathbf{y}/\partial\Omega$ at $t = T$. To evaluate $\partial\mathbf{y}/\partial\Omega$, we differentiate Eq. (15) and the initial condition $\mathbf{y}(\boldsymbol{\eta}(0), \Omega(0)) = \boldsymbol{\eta}(0)$ with respect to Ω and obtain

$$\frac{\mathrm{d}}{\mathrm{d}t}\left(\frac{\partial\mathbf{y}}{\partial\Omega}\right) = \frac{\partial}{\partial\mathbf{y}}(\mathbf{A}\mathbf{y} + \mathbf{F})\frac{\partial\mathbf{y}}{\partial\Omega} + \frac{\partial\mathbf{F}}{\partial\Omega}, \quad \frac{\partial\mathbf{y}}{\partial\Omega}(0) = \mathbf{0}. \tag{20}$$

Integrating Eq. (20) from $t = 0$ to T, we can obtain $\partial\mathbf{y}/\partial\Omega$. However, Eq. (19) consists of $2N$ linear algebraic equations and $2N + 1$ unknowns. Therefore, to have the same number of equations as the unknowns, we introduce the arc-length equation

$$\left(\frac{\partial\boldsymbol{\eta}}{\partial s}\right)^2 + \left(\frac{\partial\Omega}{\partial s}\right)^2 = 1. \tag{21}$$

Solving Eqs. (19) and (21), we can determine the tangent vector $(\partial\boldsymbol{\eta}/\partial s, \partial\Omega/\partial s)$, then we can predict values of $\boldsymbol{\eta}$ and Ω by taking a step Δs

$$\boldsymbol{\eta} = \boldsymbol{\eta}^* + \frac{\partial\boldsymbol{\eta}}{\partial s}\Delta s \quad \text{and} \quad \Omega = \Omega^* + \frac{\partial\Omega}{\partial s}\Delta s. \tag{22}$$

Because the tangent predictor is used in Eq. (22), these predicted values must be corrected through the Newton–Raphson scheme. And the procedure described above can be carried out until the periodic solution branches are traced.

4. Numerical results and discussions

A stay cable of the Dongting Lake Bridge was chosen as an example to verify the spatial motions of the cable. The bridge is a three-tower prestressed concrete cable-stayed bridge in China. It employs three towers to support its deck through 222 stay cables, forming two main spans of 310 m each, and two side spans of 130 m each. The dimensional parameters and material properties of the sample stay cable are as follows [23]: cable span $l = 121.9$ m; inclined angle $\theta = 35.2^\circ$; diameter $D = 119$ mm; initial tension $H = 3150$ kN; elastic modulus $E = 2.0 \times 10^5$ MPa; mass per unit length $m = 51.8$ kg/m. Table 1 shows the first four natural frequencies of in-plane and out-of-plane modes. These results show perfect agreement with Irvine theory [21]. Moreover, the in-plane results are basically in agreement with the measured ones [23]. The small difference between them can be seen. The difference is due to the fact that the design value of initial tension is used to determine the natural frequencies. Obviously, the real initial tension will lead to smaller difference.

In general, the damping ratio of the cable includes the viscous damping ratio and the aerodynamic damping ratio. However, it is very difficult to obtain the aerodynamic damping ratio. Therefore, only the viscous damping ratio is considered. The measured damping ratios of the cable for the first 10 in-plane modes are very small, as shown in Ref. [23],

Table 1
Natural frequencies of the inclined cable (Hz).

In-plane mode	Present	Results of Irvine theory [21]	Full-scale measurement [23]	Out-of-plane mode	Present	Results of Irvine theory [21]	Full-scale measurement [23]
1	1.0157	1.0157	1.07	1	1.0114	1.0114	–
2	2.0229	2.0229	2.14	2	2.0229	2.0229	–
3	3.0346	3.0346	3.20	3	3.0344	3.0344	–
4	4.0459	4.0459	4.23	4	4.0459	4.0459	–

ranging from about 0.079 percent to almost 0.178 percent. The constant viscous damping ratio $\xi_{iv,w} = 0.1$ percent for all the in-plane and out-of-plane modes is chosen for numerical investigation for simplicity. To guarantee the accuracy of the solutions in this study, the first four in-plane and out-of-plane modes ($N = M = 4$) are included. Although the sine series show slow convergence rate when they are used to construct a so-called *control-oriented* model [24], these modes can lead to significantly reasonable numerical results for the inclined cable with very small sag [25]. Moreover, in order to include the contributions of all these modes, the *frc*s of the point at the $\frac{4}{9}$ span of the cable are computed.

In this study, three types of motion of the support were investigated: (1) small-amplitude motion; (2) middle-amplitude motion and (3) large-amplitude motion. Also the effects of the inclined angle on the nonlinear response are examined.

4.1. Small-amplitude motion ($z_0 = 0.0001$)

In this case, the amplitude of the support motion is assumed to be 0.0001, which corresponds to the deck/tower amplitude of 1.22 cm. Fig. 2 shows the steady-state dynamic maximum amplitudes of the transverse and vertical displacements of the inclined cable as the excitation frequency varies. Where the maximum amplitudes of the displacements are defined as

$$V_{\max} = \max_{t\in[0,T]} \left\{ \sum_{i=1}^{4} \phi_i(x) q_{iv}(t) + x z_0 \cos\theta \sin \Omega t \right\}_{x=4/9}, \quad W_{\max} = \max_{t\in[0,T]} \left\{ \sum_{i=1}^{4} \phi_i(x) q_{iw}(t) \right\}_{x=4/9}. \tag{23}$$

Overall, the *frc*s of in-plane motion are, as expected, of the hardening type in the four resonance regions, where the cubic nonlinearity due to the stretching dominates the nonlinear response. For the case of the first primary resonance region ($\Omega \approx 1.0$) considered in Fig. 2a, the *frc* of in-plane motion exhibits the nonlinear vibration characteristics with relatively simple pattern. And a narrow multi-value region of the in-plane motion due to two turning point is observed. Moreover, no non-planar motion is excited. In this study, a single cable is applied to investigate the nonlinear vibration character of stay cable subject to the support motion. Obviously, it cannot describe the interactions between the cable and deck in cable-stayed bridge. Due to the coupling between cable-dominant (local) mode and beam-dominant (global) mode in the cable-stayed beam [12], the sine functions do not accurately describe the local mode in the cable-stayed beam. In fact, when

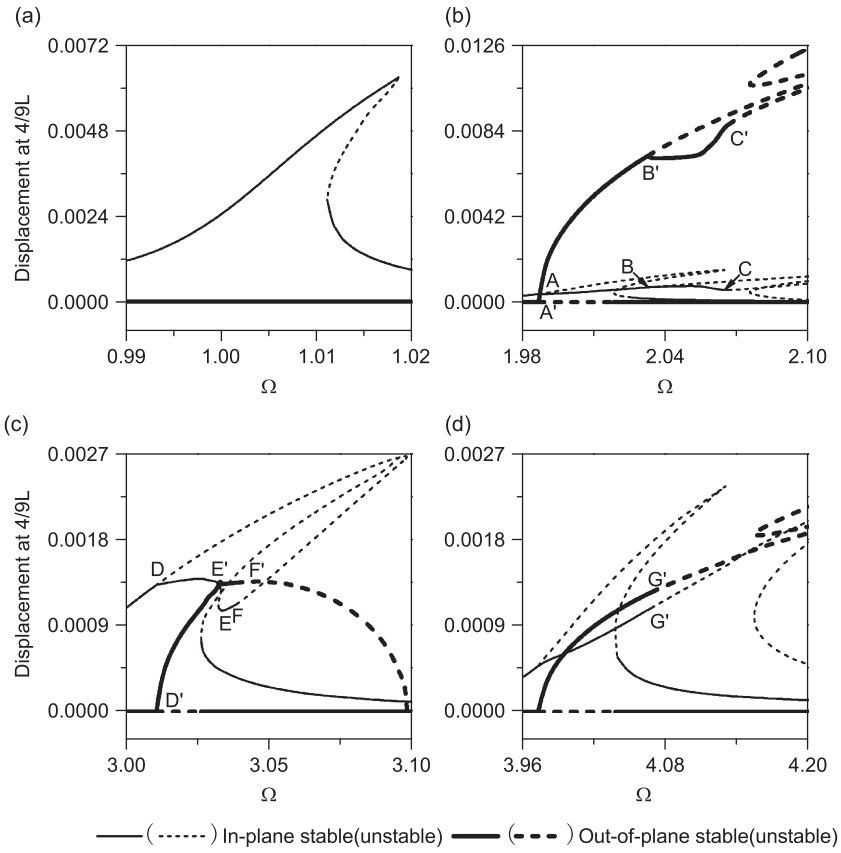

Fig. 2. Frequency–response curve of the inclined cable with $z_0 = 0.0001$: (a) $\Omega \approx 1.0$, (b) $\Omega \approx 2.0$, (c) $\Omega \approx 3.0$ and (d) $\Omega \approx 4.0$.

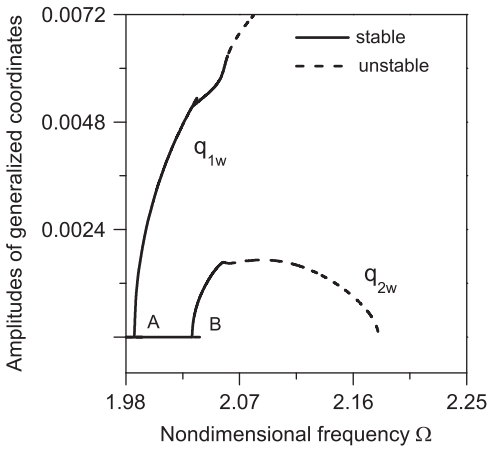

Fig. 3. The frequency–response curves of the out-of-plane modes when $\Omega \approx 2.0$.

$\Omega \approx 1.0$, the vertical motion is one-to-one resonant with first local mode, the global and local modes are strongly coupling in this case. Therefore, the hybrid modes are born as the result of combination of the global and local modes [11,12].

When the excitation frequency increases to about 2.0, significant differences of the *frc*s of in-plane and out-of-plane motions are observed (Fig. 2b). As the excitation frequency increases from 1.98, the *frc* of the cable undergoes a period-doubling bifurcation at Point A(A′) ($\Omega \approx 1.986$), which results that the planar motion loses its stability, and the nonlinear response of the cable becomes suddenly non-planar with a significant sudden increase from zero when the excitation frequency is further increased from Point C. Then a further increase in the excitation frequency Ω leads to a very rapid continuous increases in the amplitude of the out-of-plane motion, and a very slow but continuous increases in the amplitude of the in-plane motion until another bifurcation occurs at Point B(B′), where the amplitude of the out-of-plane motion is significantly larger than the amplitude of the in-plane motion. In this case, the coupling motion between in-plane motion and out-of-plane motion has become significant. Moreover, if the excitation frequency Ω further increases from this point, there exist stable non-planar motion and unstable non-planar motion simultaneously. And the amplitude of non-planar motion is nearly saturated in the frequency region $\Omega \in (2.032, 2.054)$. It is also noted that the nonlinear response of the cable will be dominated by the out-of-plane motion when the out-of-plane motion due to the period-doubling instability in the $\frac{1}{2}$ subharmonic resonance region is excited.

To better understand the relations between the bifurcation mechanisms and the coupling motion of the cable, Fig. 3 shows the amplitudes of the generalized coordinates of the out-of-plane motion as functions of the excitation frequency, where the amplitudes indicate the maximum values of the generalized coordinates attained over one excitation cycle. As seen from Fig. 3, due to the period-doubling instability at the Point A(A′), the first out-of-plane mode was indirectly excited. When the excitation frequency increases from the bifurcation Point B(B′), the second out-of-plane mode was excited. In this case, the excitation of the second out-of-plane mode is largely controlled by the nonlinear interactions due to the one-to-one internal resonance [26,27]. This case of one-to-one internal resonance of inclined cable between in-plane mode and out-of-plane mode has been investigated by Xu et al. [26] and Zhao et al. [27]. Their results showed that the one-to-one internal resonance may lead to the couple motion of inclined cable. Moreover, because the third and fourth out-of-plane modes were not excited in the $\frac{1}{2}$ subharmonic resonance region, the *frc*s of these two modes are not included in Fig. 3. It is also obvious from Fig. 3, the amplitude of the first out-of-plane mode is much larger than that of the second one, therefore, the out-of-plane motion is mainly driven by parametric resonances due to the axial inertia force.

It is very interesting to note that the stable non-planar motion loses its stability via a torus bifurcation at Point C(C′) ($\Omega \approx 2.066$) (see Fig. 2b). Thus, the non-planar motion should become quasi-periodic. To demonstrate the existence of quasi-periodic non-planar motion predicted by the current analysis, the Galerkin-discretized models are numerically integrated by employing a fourth-order Runge–Kutta method, and the initial condition for the numerical integrations are set to ones obtained by the continuation technique. Fig. 4a shows the steady-state time history of the motion at $\Omega = 2.067$. It is observed that the amplitude of time history varies with 120–150 times the excitation period. And a Poincaré section of the motion for the surface of section at $t = 0 \,(\mathrm{mod}\, 2\pi)$ is shown in Fig. 4b. The closed curve of the Poincaré section implies that the non-planar motion of the cable is quasi-periodic with the modulation frequency incommensurate with the fast frequency. Fig. 4c shows the cross-section trajectory of the point at the $\frac{4}{9}$ span of the inclined cable. As can be seen, the pattern of cross-section motion does not exhibit any symmetrical characteristic. As the excitation frequency increases from 2.061, the quasi-periodic motion undergoes a cascade of torus-doubling and the destruction of the torus (Fig. 4d–f), resulting in the chaotic non-planar motion (Fig. 4g). However, this chaotic motion only exists in a very narrow frequency range, and when the excitation frequency increases further, a jump phenomenon occurs, leading to the low amplitude planar periodic motion.

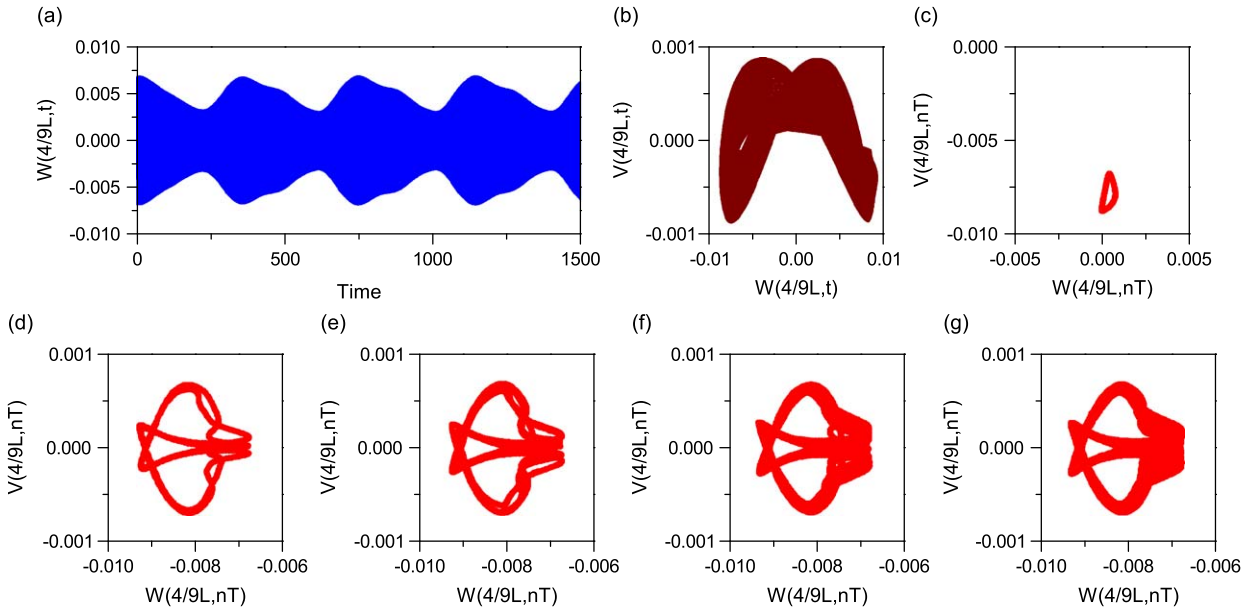

Fig. 4. The non-periodic motion of the inclined cable with $z_0 = 0.0001$: (a) time history, (b) Poincaré section, (c) cross-section trajectory when $\Omega = 2.067$; Poincaré section: (d) $\Omega = 2.069$, (e) $\Omega = 2.071$, (f) $\Omega = 2.073$ and (g) $\Omega = 2.074$.

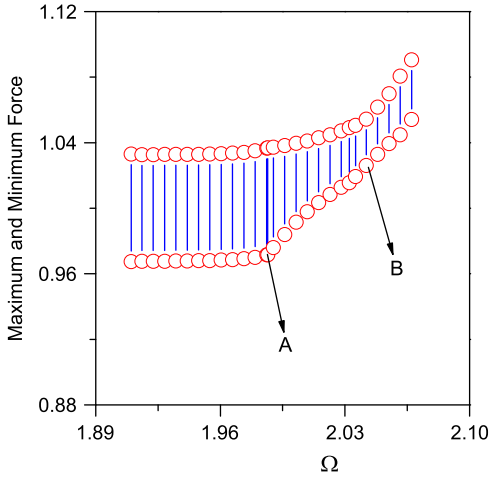

Fig. 5. Variations of the maximum and minimum axial tension with the excitation frequency.

Depending on the amplitude of the out-of-plane motion, excited by different bifurcation mechanisms, the tension of the inclined cable becomes significantly different. To investigate the relations between the tension and the bifurcation mechanisms, the non-dimensional axial total tension H_T are considered, defined as

$$H_T = 1 + \alpha z_0 \sin\theta \sin \Omega t + \alpha \sum_{i=1}^{4} q_{iv} \int_0^1 y' \phi_i'(x)\,dx + \frac{\alpha}{2} \sum_{i=1}^{4} (q_{iv} q_{iv} + q_{iw} q_{iw}) \int_0^1 \phi_i'(x) \phi_i'(x)\,dx, \tag{24}$$

where the quasi-static assumption and the orthonormality conditions of the sinusoidal mode are applied. It can be seen that the value of the axial tension does not depend on the coordinate x. This is due to the facts that we assumed that the inclined cable stretched in a quasi-static manner, and the corresponding axial inertia has been eliminated. Fig. 5 illustrates the maximum and minimum values of the axial total tension as functions of the excitation frequency. For the minimum amplitudes of the axial tension, there exist two *sharp* points, as the excitation frequency increases past the two bifurcation points. Whereas, only when the one-to-one internal resonance of the cable is excited, the *sharp* phenomena occurs on the maximum amplitudes branch of the axial tension. Through the above discussion, we can also conclude that the mean value

of the axial tension must undergo the *sharp* phenomena as different bifurcations occurs. So, to more accurately design and control the inclined cable in the engineering fields, the coupling motion of the cable should be determined. In this study, the quasi-static assumption has been applied to obtain the condensed model of the inclined cable. However, this procedure omits the nonlinear coupling of longitudinal/transversal motion of the inclined cable. In this respect, Srinil and Rega [28] has investigated the effects of the quasi-static assumption on the nonlinear dynamics of shallow cables. Their results showed that the quasi-static assumption may lead to significant quantitative and/or qualitative *discrepancies* in nonlinear dynamic and underestimated results for the axial tensions [28]. Therefore, a so-called kinematically *non-condensed* model [28] should be used to obtain more accurate axial tensions.

Fig. 2c illustrates the maximum amplitudes for the in-plane and out-of-plane motions as functions of the excitation frequency in the $\frac{1}{3}$ subharmonic resonance region ($\Omega \approx 3.0$). Globally, the *frc*s of in-plane and out-of-plane motions are similar to the ones obtained by Xu et al. [26] and Zhao et al. [27]. Therefore, the inertia force due to the transverse component of the support motion, dominates the nonlinear response of the inclined cable in this case. Referring to Fig. 2c, the out-of-plane motion due to the one-to-one internal resonance, emerges from the Point D(D′). Also the lower amplitude out-of-plane motion can be observed in the frequency region $\Omega \in (3.034, 3.045)$. This non-planar motion can lose stability via a torus bifurcation at Point F(F′), leading to a quasi-periodic motion, then a cascade of torus-doubling can be traced. However, no chaotic motion occurs as the excitation frequency increases further. Overall, the motion character and the Poincaré sections of the inclined cable for this case are very similar to the ones shown in the Fig. 4. Therefore, these results are not reported here. Compared with the peak of the in-plane motion shown in Fig. 2b, the peak does not tremendously reduce in this case. This may be due to the existence of combinational resonance such as $\Omega \approx \omega_{1v} + \omega_{2v}$, which results in the observable contribution of the first and second in-plane modes.

When the excitation frequency increases to about 4.0, Fig. 2d shows the *frc*s of the in-plane and out-of-plane cable motions when $\Omega \approx 4.0$. Similar to Fig. 2b, due to the period-doubling instability, the non-planar motion is excited. However, the fourth out-of-plane mode is not indirectly excited via the one-to-one internal resonance. And the non-planar motion loses its stability at Point G(G′).

As clear in the *frc*s of the in-plane and out-of-plane cable motions shown in Fig. 2, non-planar motion regions, where only unstable in-plane motions exist, are observed in the subharmonic resonance regions ($\Omega \approx 2.0, 3.0, 4.0$). So in these regions, the inclined cable will exhibit steady non-planar motion with any initial conditions.

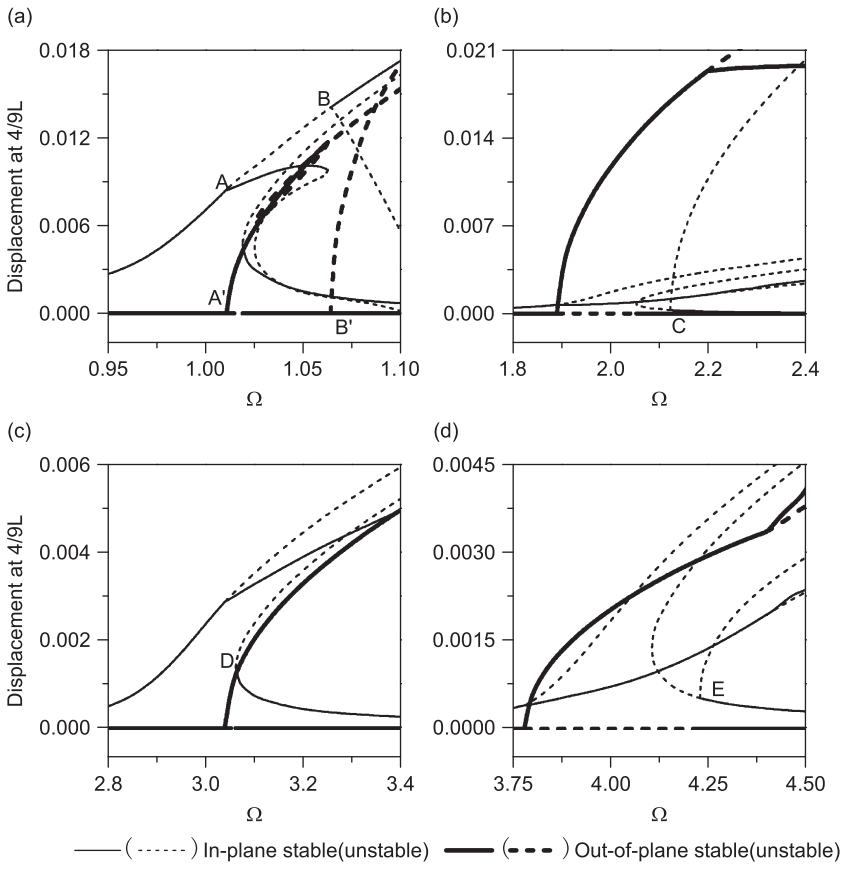

Fig. 6. Frequency–response curve of the inclined cable with $z_0 = 0.0007$: (a) $\Omega \approx 1.0$, (b) $\Omega \approx 2.0$, (c) $\Omega \approx 3.0$ and (d) $\Omega \approx 4.0$.

4.2. Middle-amplitude motion ($z_0 = 0.0007$)

Generally speaking, the amplitude of the support motion determines the cable inertial force. Therefore, the strength of the parametric resonance and primary external resonance increases as the amplitude of the support motion increases. Fig. 6 shows the *frc*s of the in-plane and out-of-plane cable motions with middle-amplitude support motion. In this case, the amplitude of the support motion is set to 0.0007. Compared with Fig. 2, the nonlinear responses induced by the middle-amplitude support motions are not very dramatically different from the ones induced by the lower-amplitude motions in the higher primary resonance regions. And significant changes of the nonlinear response of the inclined cable can be observed in the primary resonance region ($\Omega \approx 1.0$) (see Fig. 6a). In this case, due to the one-to-one internal resonance, two bifurcations of nonlinear cable response are observed at Points A(A′) and B(B′), which lead to both stable and unstable non-planar cable motions.

Referring to Fig. 6, due to the strength of the external resonance, the peaks of the in-plane and out-of-plane motions are significantly enhanced in all resonance regions, and the turning point D on the *frc* of the in-plane motion in the $\frac{1}{3}$ subharmonic resonance region (Fig. 6c) moves to left, resulting in the disappearance of the non-planar motion region. Whereas, due to the strength of the parametric resonance, the width of non-planar motion region increases in the $\frac{1}{2}$ and $\frac{1}{4}$ subharmonic resonance regions (Fig. 6b and d). It is interesting to note that the unstable in-plane motion gains its stability via a period-doubling bifurcation (Point C in Fig. 6b and Point E in Fig. 6d). And another unstable in-plane motions can emerge from these points.

4.3. Large-amplitude motion ($z_0 = 0.0014$)

To ascertain the results obtained in the case of the middle-amplitude support motion, the nonlinear response of the inclined cable subject to the large-amplitude support motion is investigated. The amplitude of the support motion used here is $z_0 = 0.0014$.

Fig. 7 shows the variations of the maximum amplitude of the in-plane and out-of-plane nonlinear responses with the excitation frequency in the resonance regions. As the amplitude of support motion increases further, the nonlinear

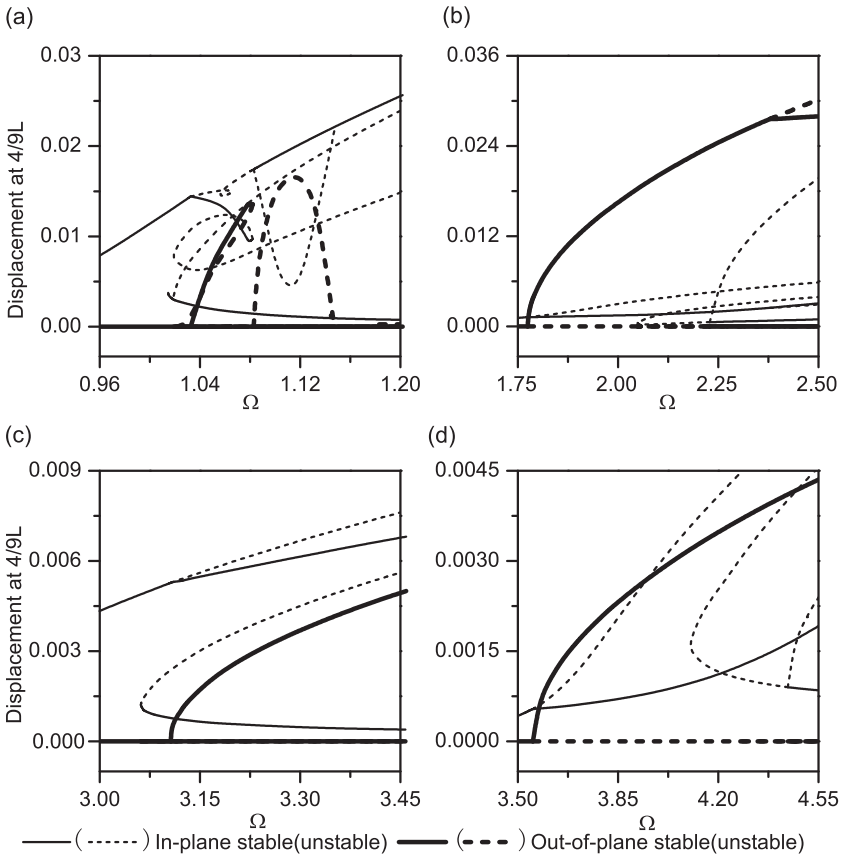

Fig. 7. Frequency–response curve of the inclined cable with $z_0 = 0.0014$: (a) $\Omega \approx 1.0$, (b) $\Omega \approx 2.0$, (c) $\Omega \approx 3.0$ and (d) $\Omega \approx 4.0$.

response characteristics of the inclined cable become more pronounced in this case. Moreover, the width of non-planar motion region increases further when the excitation frequency is close to 2.0 or 4.0 (Fig. 7b and d). However, compared with the previous case, the *frcs* still do not exhibit any significant difference, even though the amplitude of support motion is increased by 100 percent. As shown in Fig. 7a, when the stable non-planar motion in the primary resonance region ($\Omega \approx 1.0$) occurs, the amplitude of the in-plane motion decreases, whereas the one of the out-of-plane motion increases with a very fast rate as the excitation frequency increases. The reason may be attributed to the modal interaction between the in-plane motion and out-of-plane motion caused by the one-to-one internal resonance. When the strength of the modal interaction increases because the strength of the nonlinearity increases, more excitation energy is distributed to the out-of-plane motion via this modal interaction mechanism.

4.4. Effects of the incline angle

Unlike the amplitude of support motion, when the incline angle decreases, the strength of the parametric resonance decreases and the one of the external resonance increases. To investigate the effects of the incline angle, the incline angle was adjusted to 16.2°, and all other parameters of the cable remained unchanged.

Fig. 8 illustrates the *frcs* of in-plane and out-of-plane motions with the amplitude of support motion: $z_0 = 0.0001$. Compared with Fig. 2, in general, depending on the values of incline angles, the amplitude of the nonlinear response and the effects of nonlinearity become significantly different. Although the effects of the nonlinearity strengthen, the non-planar motions occur in the primary resonance region ($\Omega \approx 1.0$) (Fig. 8a), and non-planar motion regions broaden when $\Omega \approx 1.0, 3.0$.

4.5. Modal contribution ratio

The previous analysis given in the above section reveals that different modes dominate the nonlinear cable response when the coupling motions occur. To determine the relation between the degree of modal contribution and the different

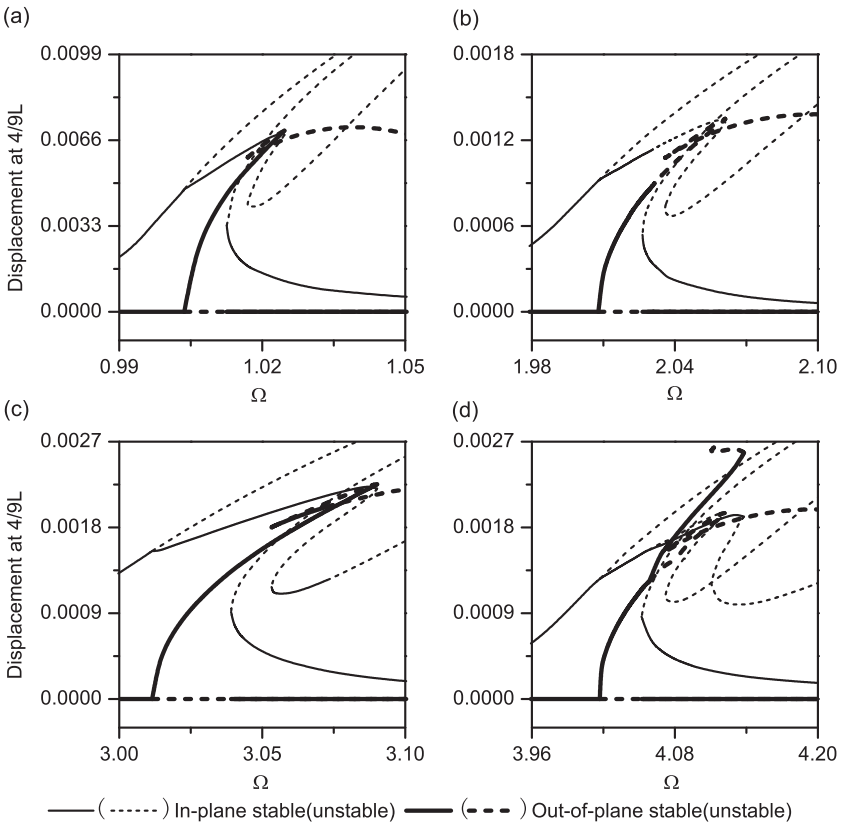

Fig. 8. Frequency–response curve of the inclined cable with $\theta = 16.2°$ and $z_0 = 0.0001$: (a) $\Omega \approx 1.0$, (b) $\Omega \approx 2.0$, (c) $\Omega \approx 3.0$ and (d) $\Omega \approx 4.0$.

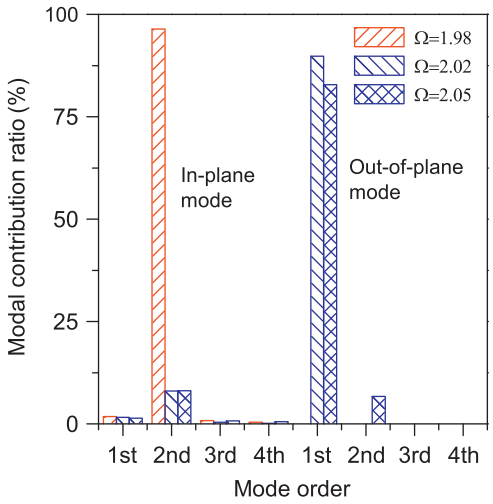

Fig. 9. The modal contribution ratio of in-plane and out-of-plane modes with $\Omega \approx 2.0$.

bifurcation mechanisms, the modal contribution ratio (MCR) is determined, defined as

$$\mathrm{MCR} = \frac{\int_0^T q_i^2(t)\,\mathrm{d}t}{\sum_{i=1}^4 \left\{ \int_0^T q_{iv}^2(t)\,\mathrm{d}t + \int_0^T q_{iw}^2(t)\,\mathrm{d}t \right\}}. \tag{25}$$

Fig. 9 shows the variation of the MCR for all the modes with different excitation frequencies in the $\frac{1}{2}$ subharmonic resonance region ($\Omega \approx 2.0$) when $z_0 = 0.0001$. It is observed from Fig. 9 that the nonlinear response is, as expected, dominated by the second in-plane mode before the period-doubling instability occurs, and the visible contribution of the first in-plane mode can be found. As the excitation frequency increases, the first out-of-plane mode governs the nonlinear response. When the second out-of-plane mode is excited via the one-to-one internal resonance, the significant contributions of the second in-plane and out-of-plane modes are observed. Clearly, the third and fourth out-of-plane modes are not indirectly excited for all the cases.

5. Conclusions

The 3-D nonlinear dynamic model of the inclined cable subject to the support motion is developed, and is applied to investigate the spatial motion of the cable. The numerical integration gives details of the non-periodic motion of the inclined cable occurring in the primary resonance region.

Numerical results have been obtained to explore the non-planar motion of the inclined cable and to examine the effects of the amplitudes of the support motion and the inclined angle on the nonlinear response of the cable. It is shown that the period-doubling instability and the nonlinear interaction due to the one-to-one internal resonance may result in the non-planar motion. They also play a significant role on the maximum and minimum values of the axial tensions. For the cable with large inclined angle, the out-of-plane motion dominates the nonlinear response when the non-planar motion due to the period-doubling instability is excited. In addition, the spatial motions of the inclined cable are much more susceptible to the inclined angle than the amplitude of the support motion.

Acknowledgments

The study was supported by National Science Foundation of China under Grant nos. 10502020 and 10772065. The first writer also acknowledge the financial support from the Hunan Science and Technology Project (no. 2008FJ3216).

Appendix A

The coefficients of Eqs. (11) and (12) are given by

$$\Gamma_{1ij} = \mathrm{i}^2 \left(1 + \alpha z_0 \sin\theta \sin \Omega t + \frac{1}{2} \alpha z_0^2 \cos^2\theta \sin^2 \Omega t \right), \quad \Gamma_{2ij} = \frac{\alpha}{\pi^2} \int_0^1 y' \phi_i'(x)\,\mathrm{d}x \int_0^1 y' \phi_j'(x)\,\mathrm{d}x,$$

$$\Gamma_{3ij} = \frac{\alpha}{2}\mathrm{j}^2 \int_0^1 y'\phi_i'(x)\,\mathrm{d}x, \quad \Gamma_{4ij} = \alpha\mathrm{i}^2 \int_0^1 y'\phi_j'(x)\,\mathrm{d}x,$$

$$\Gamma_{5ij} = \frac{\alpha}{2}\mathrm{i}^2(\mathrm{j}\pi)^2, \quad \Gamma_{6ij} = z_0\cos\theta\Omega^2 \int_0^1 x\phi_i(x)\,\mathrm{d}x - \frac{\alpha}{\pi^2} z_0 \sin\theta \int_0^1 y'\phi_i'(x)\,\mathrm{d}x,$$

$$\Gamma_{7ij} = -2\xi_i \mathrm{i} z_0 \cos\theta\Omega \int_0^1 x\phi_i(x)\,\mathrm{d}x, \quad \Gamma_{8ij} = \frac{\alpha}{2\pi^2} z_0^2 \cos^2\theta \int_0^1 y''\phi_i(x)\,\mathrm{d}x. \tag{A.1}$$

References

[1] G. Rega, Nonlinear vibrations of suspended cables. Part I: modeling and analysis, part II: deterministic phenomena, *Applied Mechanics Reviews* 57 (6) (2004) 443–479.
[2] Y. Cai, S.S. Chen, Dynamics of elastic cable under parametric and external resonances, *Journal of Engineering Mechanics* 120 (1993) 1786–1802.
[3] J.L. Lilien, A. Pinto da Costa, Vibration amplitudes caused by parametric excitation of cable stayed structure, *Journal of Sound and Vibration* 174 (1994) 69–90.
[4] A. Pinto da Costa, J.A. Martins, F. Branco, J.L. Lilien, Oscillations of bridge stay cables induced by periodic motions of deck and/or towers, *Journal of Engineering Mechanics* 122 (1996) 613–622.
[5] A. Berlioz, C.-H. Lamarque, A non-linear model for the dynamics of an inclined cable, *Journal of Sound and Vibration* 279 (2005) 619–639.
[6] C.T. Georgakis, C.A. Taylor, Nonlinear dynamics of cable stays. Part 1: sinusoidal cable support excitation, *Journal of Sound and Vibration* 281 (2005) 537–564.
[7] Z.G. Ying, Y.Q. Ni, J.M. Ko, Parametrically excited instability analysis of a semi-actively controlled cable, *Engineering Structures* 29 (2007) 567–575.
[8] T. Susumpow, Y. Fujino, Active control of multimodal cable vibrations by axial support motion, *Journal of Engineering Mechanics* 121 (1995) 964–972.
[9] Y. Fujino, P. Warnitchai, B.M. Pacheco, An experimental and analytical study of autoparametric resonance in a 3DOF model of cable-stayed-beam, *Nonlinear Dynamics* 4 (1993) 111–138.
[10] P. Warnitchai, Y. Fujino, T. Susumpow, A non-linear dynamic model for cables and its application to a cable-structure system, *Journal of Sound and Vibration* 4 (1995) 695–712.
[11] V. Gattulli, M. Morandini, A. Paolone, A parametric analytical model for nonlinear dynamics in cable-stayed beam, *Earthquake Engineering & Structural Dynamics* 31 (2002) 1281–1300.
[12] V. Gattulli, M. Lepidi, Localization and veering in cable-stayed bridge dynamics, *Computers & Structures* 85 (21–22) (2007) 1661–1668.
[13] V. Gattulli, M. Lepidi, Nonlinear interactions in the planar dynamics of cable-stayed beam, *International Journal of Solids and Structures* 40 (2003) 4729–4748.
[14] V. Gattulli, M. Lepidi, J.H.G. Macdonald, C.A. Taylor, One-to-two global-local interaction in a cable-stayed beam observed through analytical, finite element and experimental models, *International Journal of Non-linear Mechanics* 40 (2005) 571–588.
[15] Y. Xia, Y. Fujino, Auto-parametric vibration of a cable-stayed-beam structure under random excitation, *Journal of Engineering Mechanics* 132 (2006) 279–286.
[16] E. Caetano, A. Cunha, V. Gattulli, M. Lepidi, Cable–deck dynamic interactions at the International Guadiana Bridge: on-site measurements and finite element modelling, *Journal of Structural Control and Health Monitoring* 15 (3) (2008) 237–264.
[17] L. Wang, Y. Zhao, Non-linear planar dynamics of suspended cables investigated by the continuation technique, *Engineering Structures* 29 (6) (2007) 1135–1144.
[18] V. Gattulli, L. Martinelli, F. Perotti, F. Vestroni, Nonlinear oscillations of cables under harmonic loading using analytical and finite element models, *Computer Methods in Applied Mechanics and Engineering* 193 (1–2) (2004) 69–85.
[19] N.C. Perkins, Modal interactions in the non-linear response of elastic cables under parametric/external excitation, *International Journal of Non-linear Mechanics* 27 (1992) 233–250.
[20] F. Benedettini, G. Rega, A. Alaggio, Non-linear oscillations of a four-degree-of-freedom model of a suspended cable under multiple internal resonance conditions, *Journal of Sound and Vibration* 182 (1995) 775–798.
[21] H.M. Irvine, *Cable Structures*, MIT Press, Cambridge, 1981.
[22] A.H. Nayfeh, B. Balachandran, *Applied Nonlinear Dynamics*, Wiley-Interscience, New York, 1995.
[23] Y.Q. Ni, X.Y. Wang, Z.Q. Chen, J.M. Ko, Field observations of rain-wind-induced cable vibration in cable-stayed Dongting Lake Bridge, *Journal of Wind Engineering and Industrial Aerodynamics* 95 (2007) 303–328.
[24] E.A. Johnson, G.A. Baker, B.F. Spencer Jr., Y. Fujino, Semiactive damping of stay cables, *Journal of Engineering Mechanics* 133 (2007) 1–11.
[25] H.N. Arafat, A.H. Nayfeh, Non-linear responses of suspended cables to primary resonance excitations, *Journal of Sound and Vibration* 266 (2003) 325–354.
[26] Y.L. Xu, S. Zhan, J.M. Ko, Z. Yu, Experimental study of vibration mitigation of bridge stay cables, *Journal of Structural Engineering* 125 (1999) 977–986.
[27] Y.Y. Zhao, L.H. Wang, D.L. Chen, L.Z. Jiang, Nonlinear dynamic analysis of the two-dimensional simplified model of an elastic cable, *Journal of Sound and Vibration* 255 (2002) 43–59.
[28] N. Srinil, G. Rega, The effects of kinematic condensation on internally resonant forced vibrations of shallow horizontal cables, *International Journal of Non-linear Mechanics* 42 (2007) 180–195.